

Journal of Mechanics of Materials and Structures

ANISOTROPIC MULTIMATERIAL LATTICES AS THERMAL ADAPTERS

Marina M. Toropova

Volume 14, No. 1

January 2019



ANISOTROPIC MULTIMATERIAL LATTICES AS THERMAL ADAPTERS

MARINA M. TOROPOVA

Design concepts for anisotropic adaptive lattices compounded of triangular multimaterial cells are considered. The lattices connect two parts of a structure (referred here as the substrates) made of materials with different coefficients of thermal expansion (CTEs) and subject to large variation of temperature. They are designed to eliminate mismatched thermal expansion and provide constant independent of temperature distance between the substrates. Because all connections with the substrates and within the lattice are made with pins, the whole structure is free of bending and thermal expansion mismatch stresses. The designed lattices are scale independent. Relationships between cell geometry (triangle angles and height) and the CTEs of selected lattice materials are obtained. Two-cell and three-cell one-row and five-cell two-row planar lattices are designed. Furthermore, axisymmetric adaptive lattice assembly is considered. Such a lattice can have cylindrical or conical shape and may be compounded of several rows. Cell members in all designed lattices are made of conventional materials. Lattice materials providing the largest structural efficiency are recommended.

1. Introduction

Multimaterial adaptive lattices are used as connectors between two parts of a structure that are made of materials with different CTEs. If the structure experiences cyclic temperature variations, thermal expansion mismatch stresses may lead to deformations and damages [Edeson et al. 2010]. Various approaches are used to eliminate or mitigate the stresses. The first approach relates to thermal expansion mismatch adapters made of layered composite materials with graded CTE. For example, in [Yousefiani et al. 2009a; Yousefiani et al. 2009b], the authors proposed this type of adapter for a composite plate with contoured profile layers and for a layered injector-chamber attachment components in rocket engines. [Dang 2006] used composite adapters with graded CTE as components of a precision optical assembly to prevent lens misalignment. However, layered composite thermal adapters tend to accumulate residual stresses arising between the layers due to differences in the CTEs. Cyclic thermal variation amplifies the stresses and causes nonrecoverable deformations. Another approach to accommodate differential thermal expansion relates to compliant connections with low stiffness, e.g., Du et al. [2016; 2017] used flexible connections to mitigate thermal expansion mismatch deformations between a satellite platform and supporting composite rods, but this strategy reduces the overall stiffness. Multimaterial lattices do not have these drawbacks and are perfect in structures for which low weight is desirable. They are stiff and do not generate thermal expansion mismatch stresses. The lattices are compound of conventional materials and are designed in such a way that on the edges connected to the substrates, the lattice CTEs coincide with the CTEs of the corresponding substrate materials. Various thermally adaptive lattices are presented

Keywords: thermal mismatch adapters, composite cylindrical and conical lattices, multimaterial triangular cells, satellite connectors.

in [Toropova and Steeves 2014; 2015; 2016]. In these papers, the lattices are comprised of hexagonal cells with pin-joined members; three hexagon vertices are connected to an internal triangle made of a material with the CTE that differs from the hexagon material CTE. Each cell is anisotropic with three CTEs along the sides of the virtual base triangle upon which the cell is built. Such cells provide a wide range of the CTEs, but are noticeably sensitive to manufacturing imperfections in pin joints. However, the lattice design methodology elaborated in these works can be used in the design of adaptive lattices compounded of planar triangular cells that can be considered as a particular case of the hexagonal cells with zero skew angles. The triangular cells have much simpler configuration with only three pin joints, may be easily manufactured, and are much less sensitive to manufacturing imperfections compared to hexagonal cells. Three linear cell members may be made of materials with different CTEs, and the angles adjacent to the triangle base may also be different. Such cells are similar to the triangular cells used in [Grima et al. 2007a; 2007b; Miller et al. 2008; Wei et al. 2016; 2017], but have a higher degree of anisotropy, which is needed for thermal adapters. The lattices comprised of the cells are nonperiodic and the cells are nonidentical, which differs from [Sigmund and Torquato 1996; 1997; Lakes 1996; 2007; Ha et al. 2017; Gibiansky and Torquato 1997; Jefferson et al. 2009; Steeves et al. 2007; Berger et al. 2011; Berger and McMeeking 2018; Lehman and Lakes 2013; Gdoutos et al. 2013; Hopkins et al. 2013; Xu and Pasini 2016; Wei et al. 2018a]. Despite the cell's simple structure, the lattices composed of the triangular cells are able to eliminate or mitigate stresses due to different CTEs in the substrate materials.

In this paper, one-row and two-row planar lattices and multirow nonplanar axisymmetric cylindrical and conical adaptive lattices are designed. The lattices have straight-line members with pin connections to the substrates, between and within cells. Because of this, the lattices accommodate thermal deformations of the substrates without generating thermal stresses. Also, the designed lattices provide a constant temperature-independent distance between the substrates. The planar adaptive lattices may be used in multifunctional sandwich panels when they operate under variable thermal conditions, while the multirow axisymmetric adaptive lattices are used in various artificial Earth satellites as interface adapters that are not intended to bear large loads but must have optimal structural efficiency [Vasiliev et al. 2012], for example, as connectors and parts of platforms for antennas, mirrors, and other optical systems. Such nonplanar one-row axisymmetric lattices consisting of planar hexagonal cells and adapting or tuning the CTEs of two cylindrical substrates were suggested in [Toropova and Steeves 2015; 2016]. Later, the design of nonplanar lattices compounded of planar cells was developed in [Wei et al. 2018b], where planar triangular and square cells were used in lattice cylindrical shells with tailorable thermal expansion. Thermal tuning and morphing of anisotropic composite lattice shells (anisogrids) formed by clockwise and counterclockwise helical and circumferential tubular members were investigated in [Phoenix and Tarazaga 2017; 2018; Phoenix et al. 2018]. In the present work, multirow axisymmetric lattices comprised of planar triangular cells with members made of conventional materials are designed to serve as thermal adapters. The lattices can be comprised of the desirable number of cylindrical and conical rows; the cells in different rows can have different geometry and be made of different materials. However, there are no thermal expansion mismatch stresses between the rows. Relationships linking cell geometry with the CTEs of lattice cells are obtained. In contrast with conventional anisogrids, the lattices are free of bending and thermal stresses.

For all lattices presented here, the structural efficiency defined as stiffness per mass is calculated. Cell materials that provide the largest structural efficiency are indicated. The lattices are scale independent

and may be used at macro- and microscales. They do not accumulate residual stresses or display material hysteresis [Steeves et al. 2009]. Strength problems related to the lattices are not studied in the paper.

2. Formulation of the problem

Consider a structure subject to cyclic variations of temperature and consisting of two adjacent parts (referred here as the substrate one and the substrate two) made of materials with different CTEs A_1 and A_2 , respectively. If the parts are connected to each other directly, temperature variations cause mechanical stresses due to thermal expansion mismatch that can lead to nonrecoverable deformations. An anisotropic adaptive lattice that connects the two substrates and has the CTE A_1 on the edge adjacent to the substrate one and the CTE A_2 on the edge connected to the substrate two eliminates thermal expansion mismatch stresses (Figure 1).

Lattice cells have triangular shape with straight-line members that can have different lengths and be made of materials with different CTEs. Because all joints with the substrates, between cells and cell members are made with pins, the cell members can rotate and accommodate thermal expansions. The design of the adaptive lattice consists of finding angles in all cells if cell member materials are selected. Design requirements define candidates for cell materials. Then, equations linking cell geometry with material CTEs must be derived accounting for the number of rows and the number of cells in every row. The equations can be satisfied for different CTE combinations of materials-candidates providing multiple solutions to the problem. The cell member materials for which the structural efficiency is maximal are indicated.

3. Triangular anisotropic cell

In an arbitrary triangular cell, the members AB , BC , and AC (Figure 2) are made of conventional materials with Young's modulus E_i , density ρ_i , and CTE α_i , $i = 1, 2, 3$, respectively. Cell angles a and b can be different providing different member lengths $AB = L_1$, $BC = L_2$, and $AC = L_3$.

If the three member CTEs α_i , $i = 1, 2, 3$, are known, the cell geometry, i.e., the angles a and b , can be found from the conditions that the CTE along the height h is zero, the CTE along the line AB is A_1 , and the CTE along the connection line to the second substrate, which passes through the vertex C , is A_2 . Therefore, the cell geometry depends on A_1 , A_2 , and three-cell CTEs α_i , $i = 1, 2, 3$, which are

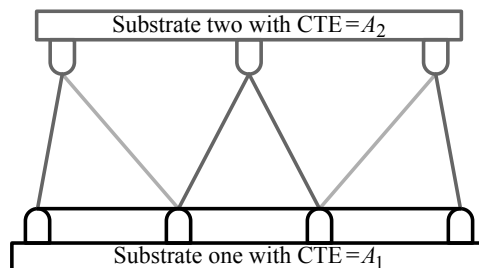


Figure 1. An example of an adaptive lattice eliminating thermal mismatch stresses between substrates with different CTEs. Lattice cell members with different CTEs are depicted with different shade of gray.

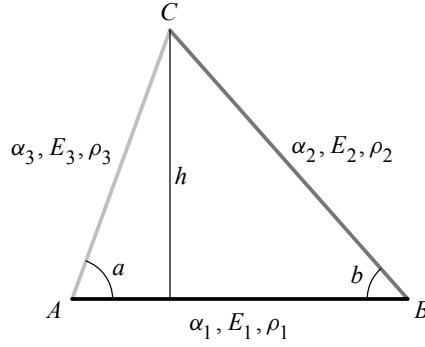


Figure 2. A lattice cell ABC with angles a and b . The members AB , BC , and AC are made of materials with CTE α_i , Young's modulus E_i , and density ρ_i , $i = 1, 2, 3$, respectively.

equal to the CTEs of selected member materials. In this work, we do not account for thermal expansion of the substrates in the vertical direction. This problem was considered in [Toropova and Steeves 2016]. Because different choices of member materials for given A_1 , A_2 determines different cell geometry, it is important to select the cell materials that provide the largest structural efficiency, i.e., stiffness per mass. For anisotropic cells compound of external hexagons and internal triangles, the structural efficiency under uniaxial loading was found in [Toropova and Steeves 2015]. A similar approach is used here to find the structural efficiency of the triangular cell under a vertical force N applied to the vertex C . The forces in the members AB , BC , AC are equal, respectively:

$$F_1 = N \frac{\cos a \cos b}{\sin(a+b)}, \quad F_2 = -N \frac{\cos a}{\sin(a+b)}, \quad F_3 = -N \frac{\cos b}{\sin(a+b)}.$$

The vertical deflection of the cell in vertex C where the force N is applied is

$$\delta = \frac{N}{\sin^2(a+b)} \left[\frac{L_1}{\Lambda_1 E_1} \cos^2 a \cos^2 b + \frac{L_2}{\Lambda_2 E_2} \cos^2 a + \frac{L_3}{\Lambda_3 E_3} \cos^2 b \right],$$

where Λ_i , $i = 1, 2, 3$, are cross-sectional areas of the members AB , BC , AC , respectively. The structural stiffness S_u under uniaxial loading can be expressed as

$$S_u = \frac{Nh}{\delta L_1}.$$

Then, the nondimensional structural efficiency P is equal to

$$P = \frac{\rho_1 S_u}{E_1 M} = \frac{\rho_1}{E_1} \frac{h \sin^2(a+b)}{L_1 \left[\frac{L_1}{\Lambda_1 E_1} \cos^2 a \cos^2 b + \frac{L_2}{\Lambda_2 E_2} \cos^2 a + \frac{L_3}{\Lambda_3 E_3} \cos^2 b \right] M}, \quad (3-1)$$

where the mass M per unit area of the lattice is

$$M = \frac{\rho_1 \Lambda_1 L_1 + \rho_2 \Lambda_2 L_2 + \rho_3 \Lambda_3 L_3}{L_1 h}. \quad (3-2)$$

Taking into account (3-2), Equation (3-1) can be rewritten as

$$P = \left(\frac{h}{L_1}\right)^2 \frac{\sin^4(a+b)}{D}, \quad (3-3)$$

where

$$D = [\sin(a+b) + Q_1 \sin a + Q_2 \sin b][\sin(a+b) \cos^2 a \cos^2 b + Q_3 \cos^2 a \sin a + Q_4 \cos^2 b \sin b],$$

$$Q_1 = \frac{\rho_2 \Lambda_2}{\rho_1 \Lambda_1}, \quad Q_2 = \frac{\rho_3 \Lambda_3}{\rho_1 \Lambda_1}, \quad Q_3 = \frac{E_1 \Lambda_1}{E_2 \Lambda_2}, \quad Q_4 = \frac{E_1 \Lambda_1}{E_3 \Lambda_3}.$$

From (3-3), we see that P increases when $a \rightarrow \frac{1}{2}\pi$ or $b \rightarrow \frac{1}{2}\pi$ and decreases when $a \rightarrow 0$ or $b \rightarrow 0$; the structural efficiency reduces when coefficients Q_i , $i = 1, 4$, containing physical constants of member materials increase. In a particular case, when the angles $a = b$ and all members have the same cross-sectional areas and are made of the same material, the nondimensional structural efficiency is equal to

$$P = \frac{\sin^4 a}{(\cos a + 1)(\cos^3 a + 1)}.$$

If, for example, $a = b = 60^\circ$, then $P = \frac{1}{3}$, which is identical with the maximal structural efficiency for the triangular lattice with equilateral cells found in [Steeves et al. 2007]. If $a = b = 70^\circ$, $P = 0.5587$; for $a = b = 80^\circ$, $P = 0.7973$. Thus, cells with larger angles a and b are preferable in terms of structural efficiency.

4. Planar lattices

In this section, stretch dominated two-cell and three-cell one-row lattices and a five-cell two-row lattice compounded of triangular cells are considered. All the lattices have a vertical line of symmetry. For two-cell and three-cell lattices the relationships connecting cell angles with member material CTEs are derived using the condition of constant, temperature-independent lattice height and kinematic conditions on the lattice edges connected to the substrates. Then, it is shown how the relationships are modified if these two lattices are combined into a five-cell two-row lattice. For lattices of more complicated shape or lattices without the vertical line of symmetry, the relationships between cell geometry and material CTEs can be derived in similar way. Lattice design starts with the selection of cell lateral side materials, and then cell angles are found. In all cells, the triangle base side material coincides with the first substrate material to exclude thermal expansion mismatch.

4A. Two-cell lattices. Let a two-cell lattice (Figure 3) be connected to the first substrate with the CTE A_1 along the line AB and to the second substrate with the CTE A_2 along the line CE , and α_{AD} , α_{DB} , and α_h denote the CTEs along AD , DB , and the height h , respectively. Because $\alpha_h = 0$,

$$\alpha_{AD} = \frac{\alpha_3}{\cos^2 a}, \quad \alpha_{DB} = \frac{\alpha_2}{\cos^2 b}.$$

The distance CE between the vertex C and the lattice line of symmetry must thermally expand with the CTE A_2 , hence

$$\cos b = \sqrt{\alpha_2/A_2} \quad (4-1)$$

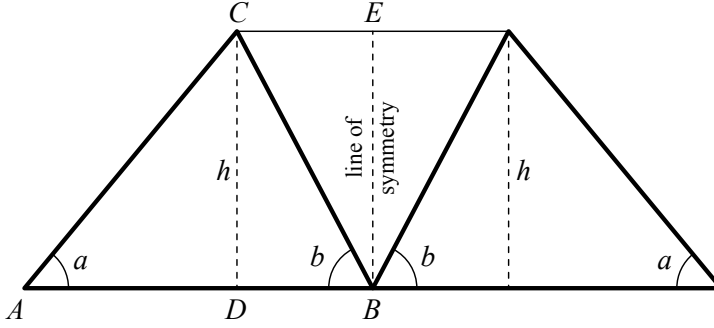


Figure 3. Two-cell lattice with a line of symmetry and a distance h between substrates.

and $\alpha_2 < A_2$. The distance between vertices A and B must expand with CTE A_1 , so

$$\frac{\alpha_3}{\sin a \cos a} - A_1 \cot a = (A_1 - A_2) \cot b. \quad (4-2)$$

The angles a and b can be found from (4-1) and (4-2) as

$$a = \frac{1}{2} \left[\arccos \left(\frac{2\alpha_3 - A_1}{w_1} \right) + \phi_1 \right], \quad b = \arccos \sqrt{\alpha_2 / A_2}, \quad (4-3)$$

where

$$w_1 = \sqrt{A_1^2 + \frac{\alpha_2}{A_2 - \alpha_2} (A_1 - A_2)^2}, \quad \phi_1 = \arccos \frac{A_1}{w_1}. \quad (4-4)$$

The second equation in (4-3) shows that the angle b rises when α_2 decreases and A_2 increases. From (4-2), it is seen that the angle a depends on the angle b and the CTE α_3 . Therefore, the first equation in (4-3) shows that if the angle b is found, then the angle a is greater for a greater difference $A_1 - 2\alpha_3$, i.e., for a smaller CTE α_3 .

4B. Three-cell lattices. Let a three-cell lattice (Figure 4) be connected to the first substrate with the CTE A_1 along the line AD and to the second substrate with the CTE A_2 along the line CE . The lattice has a vertical line of symmetry so that the angles in the middle cell $a_2 = b_2$ (Figure 4). To define lattice geometry, we have to find relationships between cell angles a_1, b_1 (related to the left cell), the angles $a_2 = b_2$ and the material CTEs $A_1, A_2, \alpha_{1i}, i = 1, 2, 3$, and $\alpha_{2j}, j = 1, 2, 3$, where $\alpha_{11}, \alpha_{12}, \alpha_{13}$ are the material CTEs of the members AB, BC, AC , respectively, and $\alpha_{21}, \alpha_{22}, \alpha_{23}$ are the material CTEs of the members BD, DE , and BE , respectively.

Repeating the procedure applied in the subsection above, we find

$$\begin{aligned} \cos^2 a_2 &= \frac{\alpha_{23}}{A_1}, \\ \frac{\alpha_{12}}{\sin b_1 \cos b_1} - A_2 \cot b_1 &= (A_2 - A_1) \cot a_2, \\ \frac{\alpha_{13}}{\sin a_1 \cos a_1} - A_1 \cot a_1 &= \left(A_1 - \frac{\alpha_{12}}{\cos^2 b_1} \right) \cot b_1. \end{aligned} \quad (4-5)$$

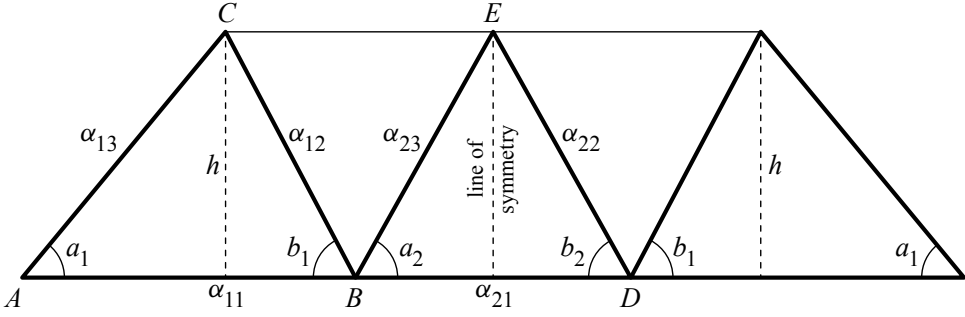


Figure 4. Designation of CTEs in a three-cell lattice with a line of symmetry and a distance h between substrates.

The solutions to the equations (4-5) can be presented as

$$\begin{aligned} a_2 = b_2 &= \arccos \sqrt{\frac{\alpha_{23}}{A_1}}, \\ b_1 &= \frac{1}{2} \left[\arccos \frac{2\alpha_{12} - A_2}{w_2} + \phi_2 \right], \\ a_1 &= \frac{1}{2} \left[\arccos \frac{2\alpha_{13} - A_1}{w_3} + \phi_3 \right], \end{aligned} \quad (4-6)$$

where $\alpha_{23} < A_1$ and

$$w_2 = \sqrt{A_2^2 + \frac{\alpha_{23}}{A_1 - \alpha_{23}} (A_1 - A_2)^2}, \quad \phi_2 = \arccos \frac{A_2}{w_2}, \quad (4-7)$$

$$w_3 = \sqrt{A_1^2 + \cot^2 b_1 \left(A_1 - \frac{\alpha_{12}}{\cos^2 b_1} \right)^2}, \quad \phi_3 = \arccos \frac{A_1}{w_3}. \quad (4-8)$$

Equations (4-5) show that the angle b_1 depends on the angle a_2 , and the angle a_1 depends on the angle b_1 . From (4-6)–(4-8) it follows that smaller values of α_{23} lead to larger values of the angle a_2 . When a_2 is found, the angle b_1 is larger for a smaller α_{12} , and for the found values of a_2 and b_1 the angle a_1 is larger for a smaller α_{13} .

4C. Five-cell two-row lattice. The lower row in a five-cell two-row lattice is designed as if it connects two substrates with the same CTE A_1 (Figure 5).

In this case, (4-6) are transformed into

$$a_1 = \arccos \sqrt{\frac{\alpha_{13}}{A_1}}, \quad b_1 = \arccos \sqrt{\frac{\alpha_{12}}{A_1}}, \quad a_2 = b_2 = \arccos \sqrt{\frac{\alpha_{23}}{A_1}}, \quad (4-9)$$

where $\alpha_{1i} < A_1$, $i = 2, 3$, and $\alpha_{11} = A_1$, α_{12} , α_{13} are the CTEs pertaining to the left cell in the lower row and the CTEs $\alpha_{21} = A_1$, $\alpha_{22} = \alpha_{23}$ relate to the middle cell in the lower row. For the angles in the upper

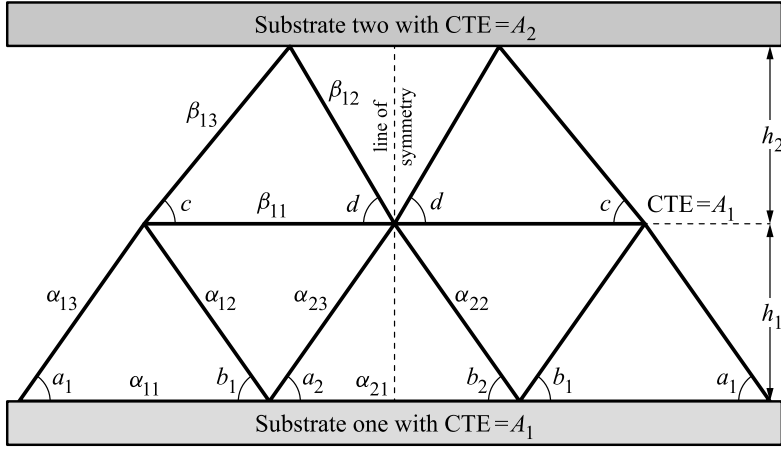


Figure 5. Designation of CTEs in a two-row five-cell lattice with a line of symmetry; the height of the first row is h_1 and the height of the second row is h_2 .

row cells, (4-3) can be rewritten as

$$c = \frac{1}{2} \left[\arccos \left(\frac{2\beta_{13} - A_1}{w_1} \right) + \phi_1 \right], \quad d = \arccos \sqrt{\frac{\beta_{12}}{A_2}}, \quad (4-10)$$

$$w_1 = \sqrt{A_1^2 + \frac{\beta_{12}}{A_2 - \beta_{12}} (A_1 - A_2)^2}, \quad \phi_1 = \arccos \frac{A_1}{w_1},$$

where the angles c , d , and the CTEs $\beta_{11} = A_1$, β_{12} , and β_{13} relate to the left cell in the upper row, and $\beta_{12} < A_2$. Note, that in a two-row lattice, the rows can have different heights $h_1 \neq h_2$, which are independent of temperature changes.

Expressions (4-3), (4-6), (4-9), and (4-10) obtained in this section are scale independent and present the cell angles as functions of A_1 , A_2 , and the CTEs of the cell member materials.

5. Examples of lattice design

In the examples considered in this paper, the first substrate is made of aluminum (CTE = 22.2 ppm/°C, Young's modulus $E = 70$ GPa, density $\rho = 2.7$ kg/m³), while the second substrate is made of titanium (CTE = 8.6 ppm/°C, Young's modulus $E = 116$ GPa, density $\rho = 4.5$ kg/m³). For lattice design, we have to select cell member materials and then find cell geometry. Because the first substrate is made of aluminum, the cell base members are also made of aluminum. Let possible candidates for the cell lateral member materials be titanium, Kovar (CTE = 5.5 ppm/°C, Young's modulus $E = 138$ GPa, density $\rho = 8.0$ kg/m³), and Invar (CTE = 1.2 ppm/°C, Young's modulus $E = 140$ GPa, density $\rho = 8.1$ kg/m³). These materials are selected because they are conventional in aerospace applications. In other design problems, different materials can be considered. Having the relationships (4-3), (4-6), (4-9), and (4-10) derived in the previous section, we can find cell geometry for two-cell and three-cell one-row lattices and five-cell two-row lattices. Here, the cell angles are found for different combinations of titanium, Kovar, and Invar for cell members. The structural efficiency calculated under uniaxial loading using (3-3)

line #	α_2 (ppm/°C)	α_3 (ppm/°C)	a	b	P
1	1.2	8.6	58.2°	68.1°	0.3631
2	1.2	5.5	66.6°	68.1°	0.3842
3	1.2	1.2	81.9°	68.1°	0.4453
4	5.5	8.6	69.7°	36.9°	0.1697
5	5.5	5.5	76.2°	36.9°	0.2010

Table 1. Angles and structural efficiency of cells in two-cell lattices connecting aluminum and titanium substrates; lateral cell members are made of different combinations of titanium, Kovar, and Invar materials.

depends on the cell angles, which depend on the cell material CTEs. The coefficients Q_i , $i = 1, 2, 3, 4$, reflecting the cell material physical properties, act as parameters. The structural efficiency of the whole lattice is equal to the minimum structural efficiency among all cells.

5A. Two-cell lattice. The structural efficiency and the angles in two-cell lattices calculated by (4-3) and (4-4) for member materials with CTEs α_2 and α_3 are shown in Table 1. It is seen that the lattice with cells made of Invar lateral and aluminum base sides and the angles $a = 81.9^\circ$, $b = 68.1^\circ$ (line 3) has the largest structural efficiency $P = 0.4453$. The presence of smaller angles b (lines 4, 5) noticeably reduces the structural efficiency.

5B. Three-cell lattice. Let P_1 and P_2 denote the structural efficiency of the left and the middle lattice cells (Figure 4), respectively. According to Table 2, the left cell made of the left titanium and the right Invar lateral sides has the structural efficiency $P_1 = 0.2947$, and the middle cell with Invar lateral sides has the structural efficiency $P_2 = 0.5401$ (line 3). Hence, the structural efficiency of the whole lattice is $P = 0.2947$, which is the largest among all other three-cell lattices with different combinations of cell member materials (lines 1, 2, 4, 5, 6) but significantly lower than the structural efficiency of the two-cell lattice connecting substrates made of the same materials. In general, analysis shows that the more cells the adaptive lattice comprises, the more the cells differ from isosceles triangles and as a result the total lattice structural efficiency reduces. In all lines of Table 2, $P_2 > P_1$, this is because the geometry of the middle cell in the designed lattice does not depend on A_2 . Therefore, a lattice connecting two substrates with the same CTEs has the maximum structural efficiency.

5C. Five-cell two-row lattice. It is possible to increase the structural efficiency of a three-cell lattice by transforming it into a five-cell two-row lattice with an additional upper row consisting of two cells. In this case, the first row of the five-cell two-row lattice is designed as if it connects two substrates with the same CTE and the lateral members are made of the same material. Hence, the triangular cells in the first row have the same angles $a_i = b_i$, $i = 1, 2$. Table 3 contains the cell angles $a_i = b_i = a$ and the structural efficiency of the cells calculated for lateral member materials with CTEs $\alpha_{12} = \alpha_{13} = \alpha_{23}$. It is seen that cells with Invar lateral sides have the largest structural efficiency $P = 0.5401$.

The upper row of the lattice coincides with the two-cell lattice designed earlier. Table 1 shows that cells with Invar lateral sides and aluminum base side have the largest structural efficiency $P = 0.4453$, which is less than 0.5401. Hence, the total lattice structural efficiency, which is identical with the structural

line #	α_{12} (ppm/°C)	α_{13} (ppm/°C)	α_{23} (ppm/°C)	a_1	b_1	a_2	P_1	P_2
1	1.2	8.6	8.6	76.4°	32.6°	51.5°	0.1751	0.1943
2	1.2	8.6	5.5	73.0°	40.0°	60.2°	0.2099	0.2593
3	1.2	8.6	1.2	65.3°	55.9°	76.6°	0.2947	0.5401
4	5.5	8.6	8.6	82.6°	14.3°	51.5°	0.0830	0.1911
5	5.5	8.6	5.5	80.6°	17.9°	60.2°	0.0995	0.2593
6	5.5	8.6	1.2	75.5°	27.1°	76.6°	0.1357	0.5401

Table 2. Angles and structural efficiency of cells in three-cell lattices connecting aluminum and titanium substrates; lateral cell members are made of different combinations of titanium, Kovar, and Invar materials.

line #	$\alpha_{12} = \alpha_{13} = \alpha_{23}$ (ppm/°C)	$a_1 = b_1 = a_2 = a$	P
1	8.6	51.5°	0.1943
2	5.5	60.2°	0.2593
3	1.2	76.6°	0.5401

Table 3. Angles and structural efficiency of cells in the first row of five-cell two-row lattices; lateral cell members are made of titanium, Kovar, and Invar materials as if they connect two aluminum substrates.

efficiency of the two-cell lattice, is attained if the cell lateral sides in both rows are made of Invar and the base sides of aluminum. A sketch of the kinematics of the lattice is shown in [Figure 6](#) where the lattice edges connected to the aluminum and titanium substrates thermally expand with the CTE of aluminum and titanium, respectively.

Three examples presented in this section demonstrate that cell lateral sides made of materials with smaller CTEs lead to larger angles adjacent to the triangle base side, and the cells with the larger angles have the larger structural efficiency even if the lateral side materials have a larger density. Note that if $A_1 > A_2$, hexagonal cells [[Toropova and Steeves 2014; 2015](#)] cannot be used in planar thermally adaptive lattices because in this case the range of their CTEs [[Toropova and Steeves 2016](#)] is not wide enough for adapting purposes.

6. Axisymmetric lattices

In this section, we consider cylindrical and conical axisymmetric lattices. Such lattices can be used in satellite structures as connectors between the main satellite body and an outboard platform. Here, the two substrates are simulated as circular disks with radii R_1 and R_2 , respectively. The lattices may consist of one or more rows of different heights, so that a desirable total distance between the substrates can be attained by combination of different rows ([Figure 7](#)).

We assume that every row has a lower and an upper circular boundary, which are virtual, so that the cells in every row are connected to the virtual lower circle with radius r_i and to the virtual upper circle with radius r_{i+1} , and $r_1 = R_1$, $r_{m+1} = R_2$ where m is the total number of rows. To form a smooth

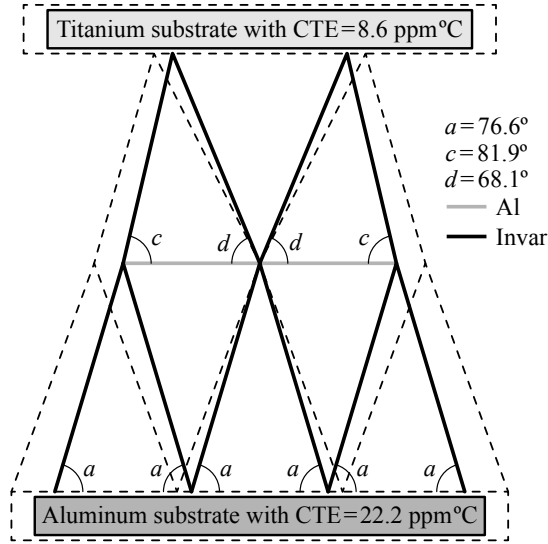


Figure 6. Sketch of the kinematics of the thermal expansion of the two-row five-cell lattice with aluminum cell base sides and Invar lateral sides. The cells with the angles $a = 76.6^\circ$, $c = 81.9^\circ$, $d = 68.1^\circ$ provide the largest structural efficiency of the lattice $P = 0.4453$ for the selected materials. The solid lines show the initial positions of the lattice, while the dashed lines show the lattice configuration and substrates after thermal changes. Note that the height of every row does not change with temperature.

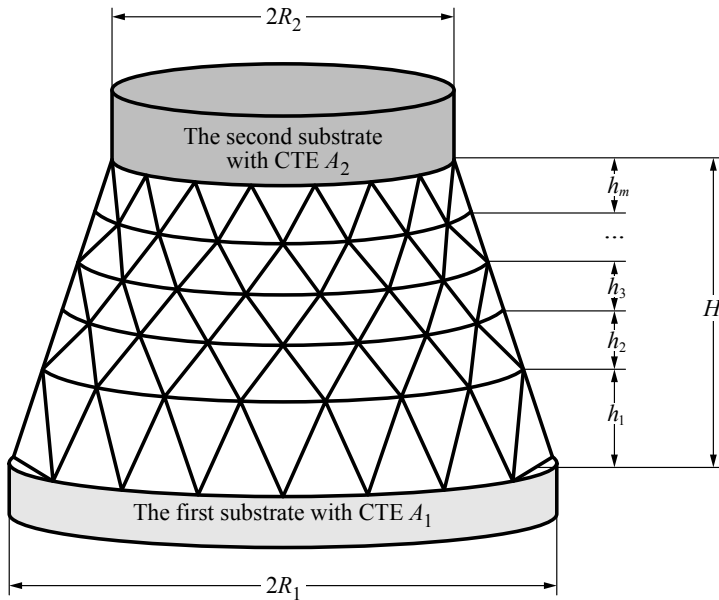


Figure 7. An example of an axisymmetric adaptive lattice consisting of m rows and connecting two circular disks with CTEs A_1 and A_2 and radii R_1 and R_2 , respectively. The distance between the substrates is H , while the height of every row is h_i , $i = \overline{1, m}$.

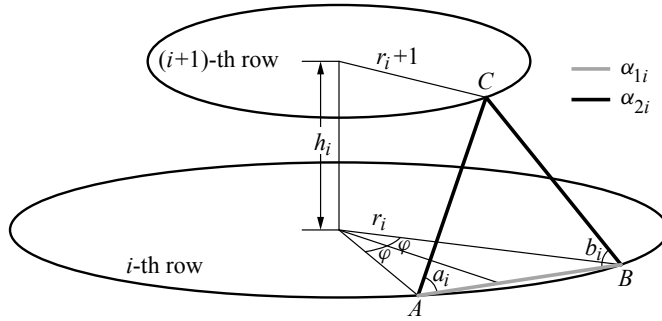


Figure 8. An axisymmetric lattice cell ABC in the i -th row. r_i and r_{i+1} are the radii of the lower and the upper row boundaries, respectively; h_i is the row height; the angle $\phi = \pi/n$, where n is a number of cells in every row. The base side AB is made of a material with the CTE α_{1i} , while the lateral sides AC and BC are made of a material with CTE α_{2i} . The cell angles at the base triangle side are equal to each other $a_i = b_i$.

cylindrical or conical surface, all rows have the same slope: $(r_i - r_{i+1})/h_i = \text{constant} = \gamma$, $i = \overline{1, m}$. In every row, there are the same number of cells and all cells have the same geometry and combination of materials that may differ from the cells in other rows. Different rows can have different heights, which remain independent of temperature, and the total distance $H = h_1 + h_2 + \dots + h_m$ between the two substrates (Figure 7) also stays independent of temperature changes. Each cell in the i -th row is a planar straight-side triangle with the base side AB made of a material with the CTEs α_{1i} , and the lateral sides BC and AC made of materials with the CTEs α_{2i} and α_{3i} , $i = \overline{1, m}$, respectively (Figure 8). It is assumed that the cell angles a_i and b_i are equal to each other and the lateral cell sides are made of the same material, so $\alpha_{2i} = \alpha_{3i}$. Therefore, the adaptive lattice is axisymmetric. In every row, we need to know two CTEs on its lower and upper boundaries, which are denoted as B_i and B_{i+1} , respectively. Two types of lattice arrangement can be used. In the first-type lattice, the first row is designed as if it connects substrates with the CTEs A_1 and A_2 , i.e., $B_1 = A_1$ and $B_2 = A_2$ and all other rows connect substrates with the CTEs A_2 and A_2 , i.e., $B_2 = B_i = A_2$, $i = \overline{3, m+1}$. In the second-type lattice, all rows except the last one are designed as if they connect substrates with the CTEs A_1 and A_1 , i.e., $B_i = B_{i+1} = A_1$, $i = \overline{1, m-1}$ and the last row connects substrates with the CTEs A_1 and A_2 , i.e., $B_m = A_1$ and $B_{m+1} = A_2$. In every row, the height h_i and the angles $a_i = b_i$ depend on B_i , B_{i+1} , and the CTE $\alpha_{2i} = \alpha_{3i}$. Before starting lattice design, we have to specify a number n of cells in every row and a lattice slope γ . The rows are designed sequentially starting with the first row. In every row, we have to select cell materials and then find the cell angles and the row height. In conical lattices, the slope differs from zero, so in every row, a radius of the upper circle r_{i+1} must be found to be used in the design of the next row. When the rows are designed, they are arranged into a whole lattice. Among all solutions to the problem, we select the combination of lattice materials that provide the largest structural efficiency.

7. One-row design

Consider a separate row of the axisymmetric lattice. It consists of n cells that connect a lower circle with radius r_i and the CTE B_i and an upper circle with radius r_{i+1} and the CTE B_{i+1} . Repeating the

procedure described in [Toropova and Steeves 2015; 2016], the CTE of the material of the cell lateral sides can be presented in the form

$$\alpha_{2i} = \alpha_{3i} = \frac{r_i^2 B_i - r_i r_{i+1} \cos \phi (B_i + B_{i+1}) + r_{i+1}^2 B_{i+1}}{r_i^2 + r_{i+1}^2 - 2r_i r_{i+1} \cos \phi + h_i^2}, \quad (7-1)$$

where $\phi = \pi/n$. The normalized height of every row can be expressed from (7-1) as

$$\eta_i = \frac{h_i}{R_1} = \sqrt{\frac{B_i - \alpha_{2i} + q_i^2 (B_{i+1} - \alpha_{2i}) - q_i \cos \phi (B_i + B_{i+1} - 2\alpha_{2i})}{\alpha_{2i}}}, \quad (7-2)$$

where $q_i = r_{i+1}/r_i$. The angles $a_i = b_i$ between the base and the lateral sides in the cell are

$$a_i = b_i = \arccos \frac{\sin \phi}{\sqrt{1 + q_i^2 - 2q_i \cos \phi + \eta_i^2}}. \quad (7-3)$$

Now, we need to specify the CTEs B_i and B_{i+1} . Because aluminum and titanium are conventional materials for a satellite and its outboard platform, the triangle base sides in the first-row cells are made of aluminum and $\alpha_{11} = B_1$ is equal to the CTE of aluminum. For B_i and B_{i+1} , $i = \overline{2, m}$, there are three possibilities: both B_i and B_{i+1} are equal to the CTE of aluminum, both B_i and B_{i+1} are equal to the CTE of titanium, and B_i is equal to the CTE of aluminum, while B_{i+1} is equal to the CTE of titanium. The normalized height of a lattice row and the angles between the base and the lateral cell sides are found from (7-2), (7-3), which are scale independent, and shown in Figures 9–11 for $0.5 \leq q_i \leq 1$, $n = 16$. Cylindrical lattices have $q_i = 1$, while for conical lattices $q_i < 1$. The curves in the plots correspond to three possible materials of the cell lateral sides: titanium, Kovar, and Invar. The intersections of these curves with the vertical line $q_i = 1$ in left sides of Figures 9, 10, and 11 provide the values of the row heights if the lateral cell sides in the cylindrical lattice are made of titanium, Kovar, and Invar, respectively. The intersections of these curves with the vertical line $q_i = 1$ in the right sides of Figures 9, 10, and 11 provide the values of the angles at the cell base sides if the lateral cell sides are made of the same set of materials. Figure 9 relates to aluminum and titanium row boundaries, Figure 10 to both titanium row boundaries, and Figure 11 to both aluminum row boundaries.

In conical lattices, $\eta_i = -q_i/\gamma + 1/\gamma$. Hence, the intersections of the straight lines in Figures 9, 10, 11 with the curves indicate the values of the row normalized height η_i and the normalized radius q_i of the row upper boundary if the cell lateral sides are made of titanium, Kovar or Invar, respectively. These values of q_i are marked with an asterisk. In this work, all plots are built for $\gamma = 0.25$. The cell angles $a_i = b_i$ can be found in Figures 9, 10, 11 when q_i are equal to the values marked with an asterisk. It is seen (Figures 9, 11) that for $\gamma = 0.25$, the straight line does not cross the Invar curves, hence, the conic lattice rows connecting aluminum and titanium substrates or both aluminum substrates can have the cell lateral sides made of titanium or Kovar but not of Invar. In a conic lattice with a smaller slope γ , cell lateral sides made of Invar may be possible. The plots in Figure 10 contain only two curves because cells with all sides made of titanium cannot provide zero CTE along the row height.

All plots show that the smaller the CTE of the lateral-side material is, cells with larger angles $a_i = b_i$ and heights η_i are needed to adapt thermal expansion. In all plots, the curves related to Invar lateral sides lie noticeably higher than the curves related to Kovar or titanium lateral members. The influence of the cell geometry on the structural efficiency is considered in the next section.

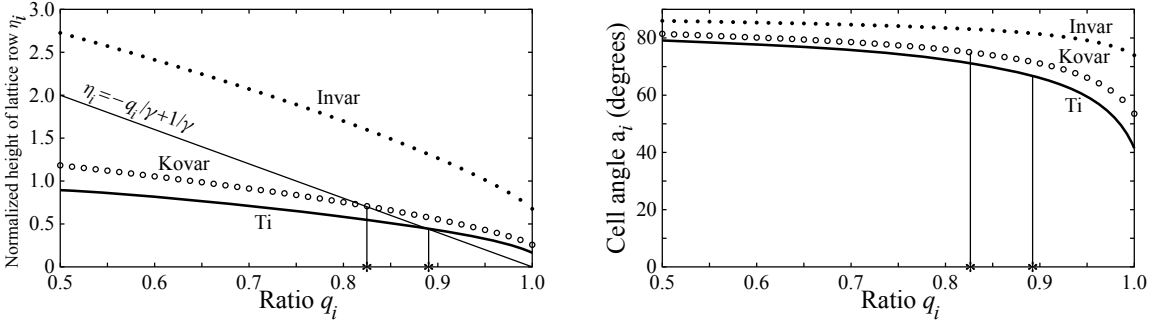


Figure 9. Normalized row height (left) and angle between the base and the lateral cell sides (right) for $B_i = 22.2 \text{ ppm}/^\circ\text{C}$, $B_{i+1} = 8.6 \text{ ppm}/^\circ\text{C}$, $n = 16$. Lateral cell side are made of Invar, Kovar, or titanium. Values of q_i with asterisks relate to conical lattices with the slope $\gamma = 0.25$.

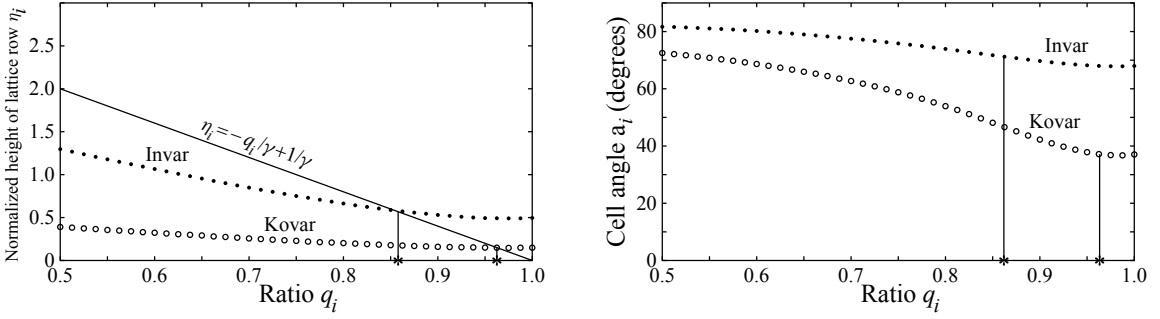


Figure 10. Normalized row height (left) and angle between the base and the cell lateral sides (right) for $B_i = B_{i+1} = 8.6 \text{ ppm}/^\circ\text{C}$, $n = 16$. Lateral cell sides are made of Invar, Kovar, or titanium. Values of q_i with asterisks relate to conical lattices with the slope $\gamma = 0.25$.

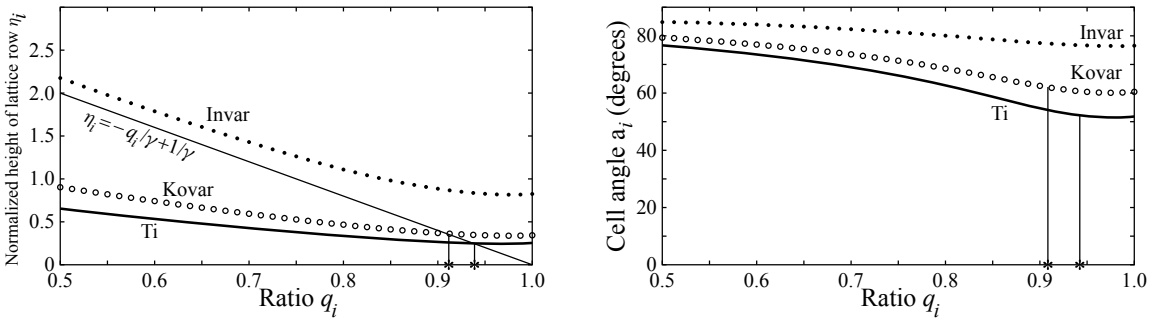


Figure 11. Normalized row height (left) and angle between the base and the cell lateral sides (right) for $B_i = B_{i+1} = 22.2 \text{ ppm}/^\circ\text{C}$, $n = 16$. Lateral cell sides are made of Invar, Kovar, or titanium. Values of q_i with asterisks relate to conical lattices with the slope $\gamma = 0.25$.

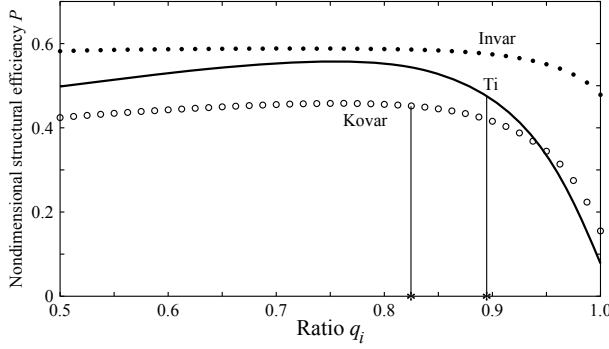


Figure 12. Nondimensional structural efficiency of a cell in axisymmetric lattice under uniaxial loading with Invar, Kovar, and titanium lateral sides for $B_i = 22.2 \text{ ppm}/^\circ\text{C}$, $B_{i+1} = 8.6 \text{ ppm}/^\circ\text{C}$, $n = 16$, $\Lambda_{1i} = \Lambda_{2i}$.

8. Structural efficiency of a cell in the axisymmetric lattice

If a cell in the axisymmetric lattice is in equilibrium when the force N is applied to its upper vertex C (Figure 8), the forces in the base and the lateral triangle sides are

$$F_1 = \frac{1}{2}N \cot a, \quad F_2 = F_3 = -\frac{N}{2 \sin a}.$$

Equation (3-3) for nondimensional structural efficiency of a cell in the axisymmetric lattice can be transformed into

$$P = \frac{\eta_i^4}{(\sin \phi + Q_1 l)(\sin^3 \phi + Q_2 l^3)},$$

where

$$l = \sqrt{1 + q_i^2 - 2q_i \cos \phi + \eta_i^2}, \quad Q_1 = \frac{\rho_{2i} \Lambda_{2i}}{\rho_{1i} \Lambda_{1i}}, \quad Q_2 = \frac{\Lambda_{1i} E_{1i}}{\Lambda_{2i} E_{2i}},$$

and Λ_{1i} , Λ_{2i} , E_{1i} , E_{2i} , ρ_{1i} , and ρ_{2i} are cross-sectional area, Young's modulus, and density of the materials of the base and the lateral cell sides, respectively. The curves describing the structural efficiency of the lattice cell with the lateral sides made of titanium, Kovar, or Invar are shown in Figures 12–14 for aluminum and titanium, both titanium, and both aluminum row boundaries, respectively. The intersections of these curves with the vertical line $q_i = 1$ provide the values of the structural efficiency of the cell in the one-row cylindrical lattice. The structural efficiency of the cell in the one-row conical lattice can be found in these figures when q_i takes the values marked with an asterisk; they coincide with the corresponding q_i marked with an asterisk in Figures 9, 10, 11. The plots are built for $\Lambda_{1i} = \Lambda_{2i}$.

The plots show that the structural efficiency depends of cell geometry, which depends on cell material CTEs. Note that the number of cells n in each row insignificantly affects the cell angles $a_i = b_i$ and the structural efficiency P , although they both slightly decrease when n increases.

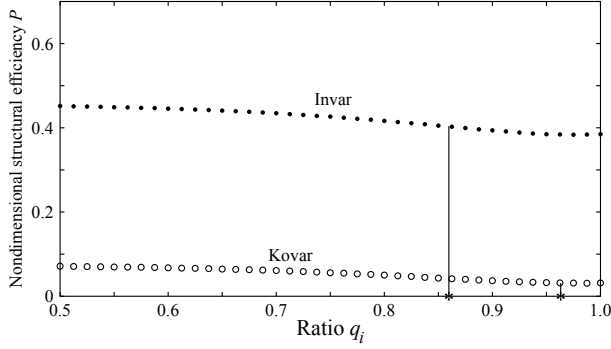


Figure 13. Nondimensional structural efficiency of a cell in axisymmetric lattice under uniaxial loading with Invar and Kovar lateral sides for $B_i = B_{i+1} = 8.6 \text{ ppm/}^\circ\text{C}$, $n = 16$, $\Lambda_{1i} = \Lambda_{2i}$.

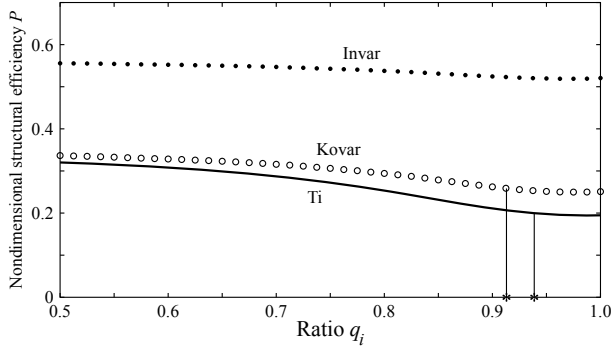


Figure 14. Nondimensional structural efficiency of a cell in axisymmetric lattice under uniaxial loading with Invar, Kovar, and titanium lateral sides for $B_i = B_{i+1} = 22.2 \text{ ppm/}^\circ\text{C}$, $n = 16$, $\Lambda_{1i} = \Lambda_{2i}$.

9. Cylindrical lattices

In cylindrical lattices $R_1 = R_2 = R$, and all lattice rows also have the same radius R . Equations (7-1)–(7-2) can be rewritten as

$$\alpha_{2i} = \alpha_{3i} = \frac{2 \sin^2(\frac{1}{2}\phi)(B_i + B_{i+1})}{4R^2 \sin^2(\frac{1}{2}\phi) + h_i^2},$$

$$\eta_i = \sin(\frac{1}{2}\phi) \sqrt{\frac{2B_i + 2B_{i+1} - 4\alpha_{2i}}{\alpha_{2i}}}. \quad (9-1)$$

Cell angles $a_i = b_i$ can be found as

$$a_i = b_i = \arccos \frac{\cos(\frac{1}{2}\phi) \sqrt{2\alpha_{2i}}}{\sqrt{B_i + B_{i+1}}}. \quad (9-2)$$

line #	B_i (ppm/°C)	B_{i+1} (ppm/°C)	$\alpha_{2i} = \alpha_{3i}$ (ppm/°C)	η_i	$a_1 = b_1$	P
1	22.2	8.6	1.2	0.67	73.9°	0.4788
2	22.2	8.6	5.5	0.26	53.5°	0.1562
3	22.2	8.6	8.6	0.17	42.0°	0.0798
4	22.2	22.2	1.2	0.82	76.6°	0.5198
5	22.2	22.2	5.5	0.34	60.3°	0.2508
6	22.2	22.2	8.6	0.25	51.7°	0.1954
7	8.6	8.6	1.2	0.49	68.2°	0.3841
8	8.6	8.6	5.5	0.15	37.3°	0.0364

Table 4. Normalized row height, cell angles, and structural efficiency in 16-cell one-row cylindrical lattices connecting two substrates with CTEs B_i and B_{i+1} corresponding to aluminum or titanium. Lines 1–3 relate to Figures 9 and 12; lines 4–6 to Figures 11 and 14; and lines 7, 8 to Figures 10 and 13; $q_i = 1$. Lateral cell sides are made of titanium, Kovar, or Invar materials.

The cylindrical lattice is assembled row by row. The total number of lattice rows depends on a desirable lattice height. Every row is designed as if it connects two circles so that the second circle material in a row and the first circle material in the next row must have the same CTE. Because A_1 and A_2 relate to aluminum and titanium, respectively, the row circle materials may be aluminum or titanium. Hence the base cell sides can be made of aluminum or titanium. Figures 9, 10, 11 show that titanium, Kovar, and Invar can be selected as cell lateral side materials if the lower and the upper circles are made of aluminum and titanium, respectively, or if the both circles are made of aluminum. For both titanium row circle boundaries, Invar and Kovar lateral cell sides are possible. Cell geometry (the angles and the normalized height) and the nondimensional cell structural efficiency under uniaxial loading obtained from (9-1) and (9-2) are shown in Table 4.

Table 4 demonstrates that cell lateral sides made of Invar provide the largest structural efficiency compared to Kovar and titanium lateral sides, which is in agreement with the data in Figures 12–14. Hence, we consider the design of the first- and the second-type adaptive lattices with Invar cell lateral sides connecting aluminum and titanium substrates, which are shown in Figures 15 and 16, respectively. Only four rows are depicted.

First-type lattice. The normalized height of the lattice's first row (line 1 in Table 4) is 0.67 and the cell base side is made of aluminum while the lateral sides are made of Invar; the cell angles are 73.9° and the structural efficiency is 0.4788. All other rows have the normalized height 0.49 (line 7 in Table 4) and are made of titanium for the base and Invar for the lateral sides; the cell angles are 68.2° and the structural efficiency is 0.3841. Hence, the lattice structural efficiency is 0.3841 and the total height is $[0.67 + (m-1)0.49]R$ (Figure 15).

Second-type lattice. The normalized height of the lattice's first $m-1$ rows is 0.82 (line 4 in Table 4), the cell base side is made of aluminum, while the lateral sides are made of Invar; the cell angles are 76.6° and the structural efficiency is 0.5198. The last row has a normalized height 0.67 (line 1 in Table 4) with aluminum base and Invar lateral cell sides, the cell angles are 73.9° and the structural efficiency is

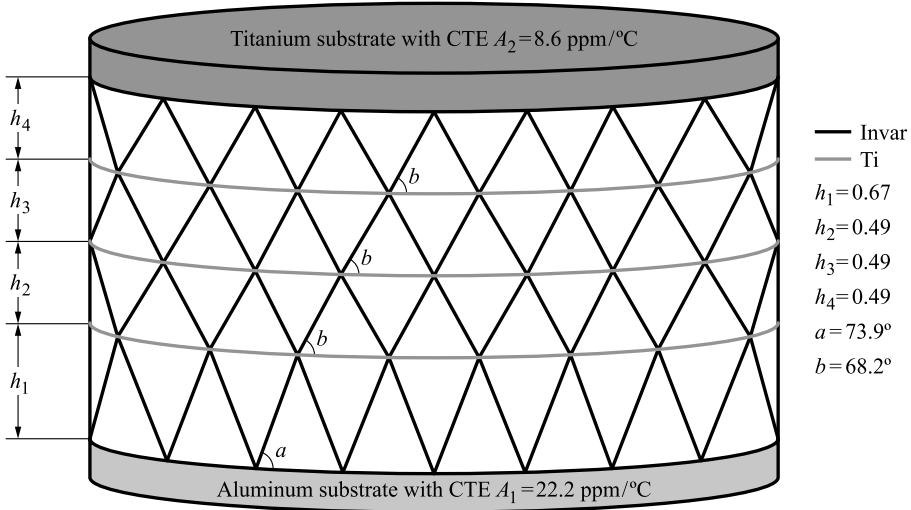


Figure 15. First-type cylindrical adaptive lattice connecting aluminum and titanium circular disks. The cell lateral members are made of Invar. In the first row, the angle at the triangle base side is $a = 73.9^\circ$ and the base members are made of aluminum, while in all other rows the angle at the triangle base side is $b = 68.2^\circ$ and the base members are made of titanium. The lattice structural efficiency is $P = 0.3841$.

0.4788. Hence, the lattice structural efficiency is 0.4788 and the total height is $[0.82(m-1) + 0.67]R$ (Figure 16), which are larger than in the first-type lattice.

It is possible to design other adaptive cylindrical lattices connecting aluminum and titanium substrates composed of cells made of Kovar or titanium lateral sides, but their structural efficiency is significantly smaller. For example, in the second-type cylindrical lattice with Kovar cell lateral sides the cell angles in the first $m-1$ rows are 60.3° (line 5 in Table 4), the heights of the rows are equal to 0.34, and the structural efficiency is 0.2508. In the last row, the angles are 53.5° (line 2 in Table 4), the height is 0.26, and the structural efficiency is 0.1562. The total structural efficiency is $\min\{0.2508, 0.1562\} = 0.1562$ and the total height is $[0.34(m-1) + 0.26]R$. Also, a first-type lattice with Kovar lateral sides is possible, but its structural efficiency is extremely low (line 8 in Table 4). A second-type lattice with all titanium lateral cell sides (line 6 and 3 in Table 4) has very small structural efficiency $\min\{0.1954, 0.0798\} = 0.0798$.

10. Conical lattices

A truncated conical lattice consists of several rows. If the lattice slope and the CTEs of the row boundaries B_i, B_{i+1} are predetermined and the lateral cell side CTEs $\alpha_{2i} = \alpha_{3i}$ are selected, the normalized radius of the upper-row circle can be expressed from (7-2) as

$$q_i = \frac{2\alpha_{2i} - w(s_{1i} + s_{2i})\gamma^2 - \sqrt{(2\alpha_{2i} - w(s_{1i} + s_{2i})\gamma^2)^2 - 4(\alpha_{2i} - s_{2i}\gamma^2)(\alpha_{2i} - s_{1i}\gamma^2)}}{2(\alpha_{2i} - s_{2i}\gamma^2)},$$

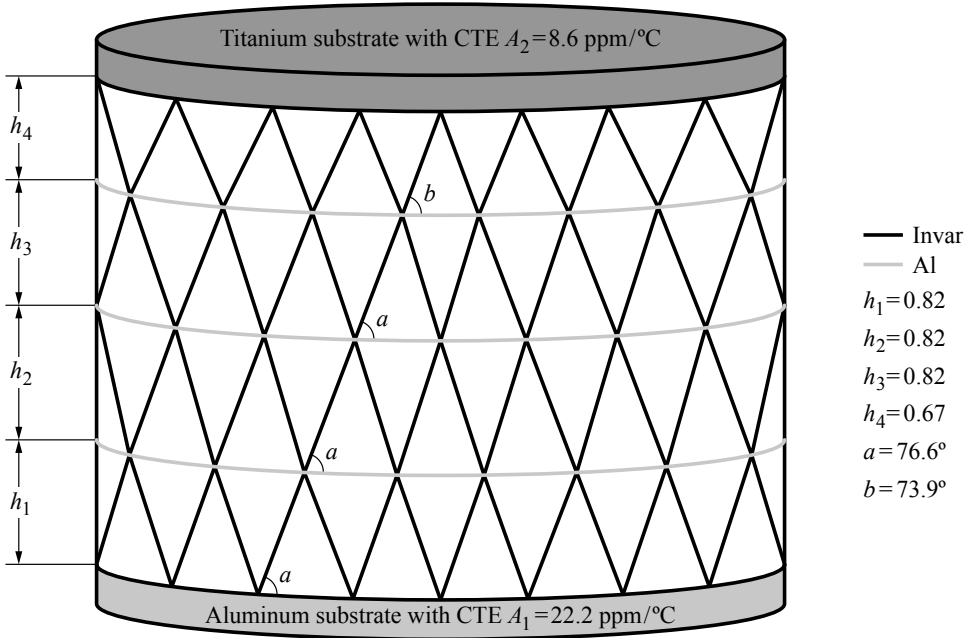


Figure 16. Second-type cylindrical adaptive lattice connecting aluminum and titanium circular disks. The cell lateral members are made of Invar, while the base members are made of aluminum. In the last row, the angle at the triangle base side is $b = 73.9^\circ$ and in all other rows the angle at the triangle base side is $a = 76.6^\circ$. Lattice structural efficiency is $P = 0.4788$.

where $s_{1i} = B_i - \alpha_{2i}$, $s_{2i} = B_{i+1} - \alpha_{2i}$, $w = \cos \phi$. The cell angles in the i -th row are

$$a_i = b_i = \arccos \frac{\sin \phi \sqrt{\alpha_{2i}}}{\sqrt{B_i + q_i^2 B_{i+1} - q_i \cos \phi (B_i + B_{i+1})}}.$$

Because the lattices designed in this work are scale independent, let $R_1 = 1$.

First-type lattices. Here, we design two first-type lattices. If $\gamma = 0.25$, then the first row of the conical lattice can have titanium or Kovar cell lateral sides (Section 8). In the next rows connecting two virtual titanium circles the cell lateral sides may be made of Kovar or Invar, but Invar is preferable because it provides larger structural efficiency. In the first row of the first lattice, the lateral and the base cell sides are made of titanium and aluminum, respectively, while in the first row of the second lattice the lateral and the base cell sides are made of Kovar and aluminum, respectively. In both lattices, starting from the second row, the cells have Invar lateral and titanium base sides. Tables 5 and 6 contain the values of the row height, the cell angles and the structural efficiency in the two first-type lattices. Both lattices can have as many rows as it is necessary for design purposes; in all following rows the cell materials and the angles will be the same as in the lines 2, 3, 4 of Tables 5 and 6. The minimum structural efficiency in both tables is the same $P = 0.3914$ but their total heights are different: $H = 178$ in the first lattice

row #	B_i (ppm/°C)	B_{i+1} (ppm/°C)	$\alpha_{2i} = \alpha_{3i}$ (ppm/°C)	h_i	$a_i = b_i$	q_i	P
1	22.2	8.6	8.6	0.46	67.2°	0.89	0.4892
2	8.6	8.6	1.2	0.51	71.6°	0.86	0.3914
3	8.6	8.6	1.2	0.44	71.6°	0.86	0.3914
4	8.6	8.6	1.2	0.37	71.6°	0.86	0.3914

Table 5. Cell angles, structural efficiency, and row heights in the first-type conical lattice consisting of four rows and connecting aluminum and titanium substrates. The cell lateral sides in the first row are made of titanium, while in other rows of Invar.

row #	B_i (ppm/°C)	B_{i+1} (ppm/°C)	$\alpha_{2i} = \alpha_{3i}$ (ppm/°C)	h_i	$a_i = b_i$	q_i	P
1	22.2	8.6	5.5	0.72	75.2°	0.82	0.4523
2	8.6	8.6	1.2	0.47	71.6°	0.86	0.3914
3	8.6	8.6	1.2	0.40	71.6°	0.86	0.3914
4	8.6	8.6	1.2	0.35	71.6°	0.86	0.3914

Table 6. Cell angles, structural efficiency, and row heights in the first-type conical lattice consisting of four rows and connecting aluminum and titanium substrates. The cell lateral sides in the first row are made of Kovar, while in other rows of Invar.

row #	B_i (ppm/°C)	B_{i+1} (ppm/°C)	$\alpha_{2i} = \alpha_{3i}$ (ppm/°C)	h_i	$a_i = b_i$	q_i	P
1	22.2	22.2	8.6	0.25	52.6°	0.94	0.1996
2	22.2	22.2	8.6	0.24	52.6°	0.94	0.1996
3	22.2	22.2	8.6	0.22	52.6°	0.94	0.1996
4	22.2	8.6	8.6	0.37	67.2°	0.89	0.4892

Table 7. Cell angles, structural efficiency, and row heights in the second-type conical lattice consisting of four rows and connecting aluminum and titanium substrates. The cell lateral sides are made of titanium.

(Figure 17) and $H = 194$ in the second lattice. Note that in conical lattices neighboring rows can have the same cell angles but row heights are different.

Second-type lattices. Two second-type conical lattices are designed here; their geometric data and the structural efficiency are shown in Tables 7 and 8, respectively. In both lattices, the base cell sides in all rows are made of aluminum. As it was shown in Section 8, second-type conical lattices cannot have cell lateral sides made of Invar. Hence, the cell lateral sides in the first lattice are made of titanium with the total structural efficiency $P = 0.1996$ and the total height $H = 108$, while the lateral sides in the second lattice are made of Kovar with the total structural efficiency $P = 0.2608$ and the total heights $H = 153$, which is noticeably smaller than for two first-type conical lattices designed earlier.

Cylindrical and conical lattice rows designed in this work can be combined in any desirable way. For example, a lattice in Figure 18 consists of a one-row cylindrical lattice and a four-row conical lattice. Both

row #	B_i (ppm/°C)	B_{i+1} (ppm/°C)	$\alpha_{2i} = \alpha_{3i}$ (ppm/°C)	h_i	$a_i = b_i$	q_i	P
1	22.2	22.2	5.5	0.36	62.13°	0.91	0.2608
2	22.2	22.2	5.5	0.33	62.13°	0.91	0.2608
3	22.2	22.2	5.5	0.30	62.13°	0.91	0.2608
4	22.2	8.6	5.5	0.54	75.23°	0.82	0.4523

Table 8. Cell angles, structural efficiency, and row heights in the second-type conical lattice consisting of four rows and connecting aluminum and titanium substrates. The cell lateral sides are made of Kovar.

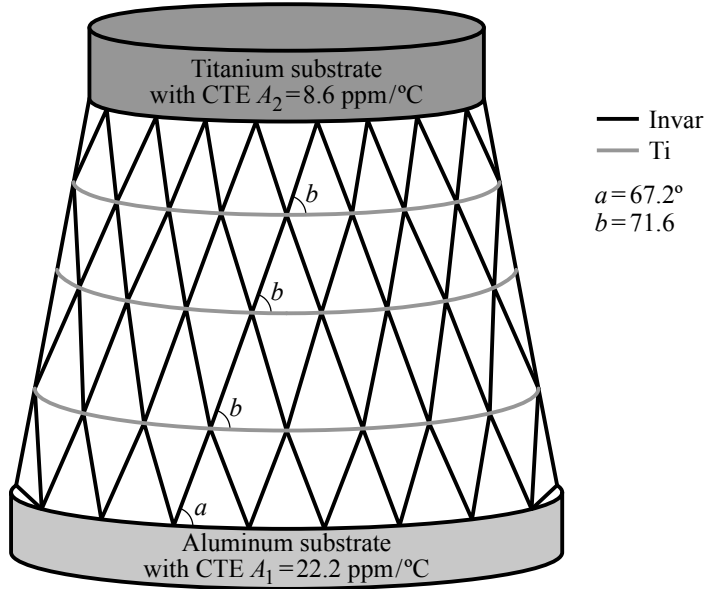


Figure 17. First-type conical adaptive lattice with Invar lateral cell members connecting aluminum and titanium circular disks. In the first row, the angle at the triangle base side is $a = 67.2^\circ$ and the base members are made of aluminum, while in all other rows the angle at the triangle base side is $b = 71.6^\circ$ and the base members are made of titanium. Lattice structural efficiency is $P = 0.3914$.

lattices in Figures 17, 18 have the same structural efficiency $P = 0.3914$. The design of axisymmetric lattices performed here demonstrates that both types of lattice arrangement can provide large structural efficiency. For example, the first row in Figure 18 belongs to the first-type, while the other rows to the second-type of lattice arrangement.

11. Conclusions

The research shows that planar triangular cells can form planar or 3-D axisymmetric cylindrical or conical anisotropic adaptive lattices connecting two substrates with different CTEs. Such lattices do not accumulate thermal stresses, provide temperature independent-distance and have high ability to eliminate

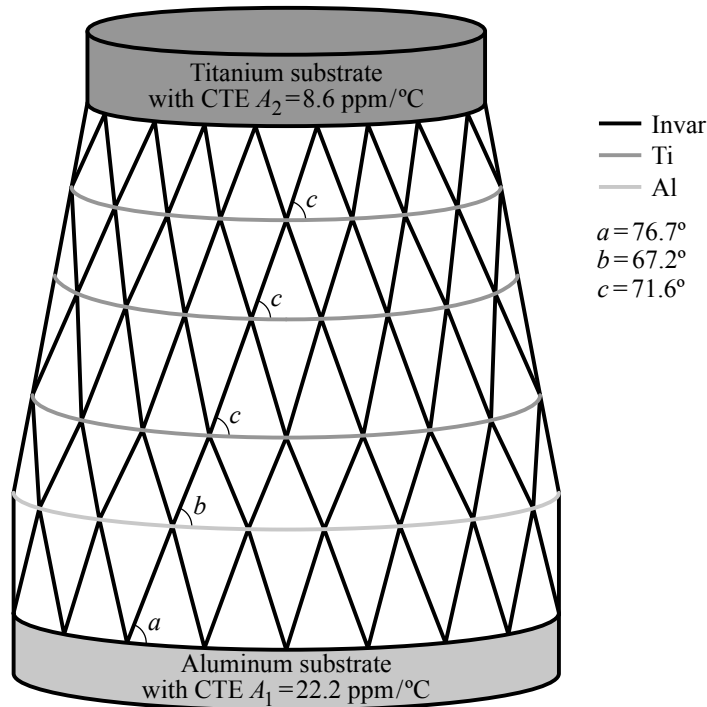


Figure 18. Five-row axisymmetric adaptive lattice combined of a one-row cylindrical lattice and a four-row conical lattice and connecting aluminum and titanium circular disks. Cell lateral sides are made of Invar. The cells in the first two rows have aluminum base sides and in all other rows - titanium base sides. The angle at the triangle base side in the first row is $a = 73.9^\circ$, in the second row is $b = 67.2^\circ$, and in all other rows $c = 71.6^\circ$. Lattice structural efficiency is $P = 0.3914$.

thermal expansion mismatch stresses between the substrates. Lattice cells are straight line triangles with different angles at the cell base sides; three-cell members are made of conventional materials with different CTEs. Nonidentical cells can be arranged in several rows of different heights. To design such a lattice, the equations linking the cell angles to the CTEs of member materials must be obtained from the kinematic constraints imposed on the lattice; their solutions are scale independent. Materials desirable for the design task with CTEs that provide the existence of a solution to these equations are considered in order to select a combination yielding the maximum structural efficiency of the lattice. The cell angles are found from the equations as functions of two substrate CTEs and the CTEs of cell materials. It is noticed that materials with smaller CTEs lead to cells with larger angles at the cell base sides, which results in larger structural efficiency of the cells under uniaxial loading. The lattices with triangular cells can connect substrates with both ratios of their CTEs $A_1 < A_2$ or $A_1 > A_2$, which is different from planar lattices with hexagonal cells (used in previous works) that can serve as adapters only when $A_1 < A_2$. Compared to the lattices with hexagonal cells the presented lattices can be easily manufactured and are more stable to manufacturing imperfections because each cell has only three joints.

References

- [Berger and McMeeking 2018] J. B. Berger and R. M. McMeeking, “Mechanical characterization of a bonded tailorable coefficient of thermal expansion lattice with near optimal performance”, *J. Mater. Res.* **33**:20 (2018), 3383–3397.
- [Berger et al. 2011] J. Berger, C. Mercer, R. M. McMeeking, and A. G. Evans, “The design of bonded bimaterial lattices that combine low thermal expansion with high stiffness”, *J. Am. Ceram. Soc.* **94**:S1 (2011), S42–S54.
- [Dang 2006] C. H. Dang, “Coefficient of thermal expansion adaptor”, US patent application US20080160274A1, 2006, <https://tinyurl.com/pat0274a1>.
- [Du et al. 2016] Z. Du, M. Zhu, Z. Wang, and J. Yang, “Design and application of composite platform with extreme low thermal deformation for satellite”, *Compos. Struct.* **152** (2016), 693–703.
- [Du et al. 2017] Z.-C. Du, H.-F. Hou, Z.-G. Wang, and J.-G. Yang, “Thermal deformation isolation for satellite platforms via flexible connections”, *Int. J. Precis. Eng. Manuf.* **18**:12 (2017), 1821–1832.
- [Edeson et al. 2010] R. Edeson, G. S. Aglietti, and A. R. L. Tatnall, “Conventional stable structures for space optics: the state of the art”, *Acta Astronaut.* **66**:1-2 (2010), 13–32.
- [Gdoutos et al. 2013] E. Gdoutos, A. A. Shapiro, and C. Daraio, “Thin and thermally stable periodic metastructures”, *Exp. Mech.* **53**:9 (2013), 1735–1742.
- [Gibiansky and Torquato 1997] L. V. Gibiansky and S. Torquato, “Thermal expansion of isotropic multiphase composites and polycrystals”, *J. Mech. Phys. Solids* **45**:7 (1997), 1223–1252.
- [Grima et al. 2007a] J. N. Grima, P.-S. Farrugia, R. Gatt, and V. Zammit, “Connected triangles exhibiting negative Poisson’s ratios and negative thermal expansion”, *J. Phys. Soc. Jpn.* **76**:2 (2007), art. id. 025001.
- [Grima et al. 2007b] J. N. Grima, P. S. Farrugia, R. Gatt, and V. Zammit, “A system with adjustable positive or negative thermal expansion”, *Proc. R. Soc. Lond. A* **463**:2082 (2007), 1585–1596.
- [Ha et al. 2017] C. S. Ha, M. E. Plesha, and R. S. Lakes, “Simulations of thermoelastic triangular cell lattices with bonded joints by finite element analysis”, *Extreme Mech. Lett.* **12** (2017), 101–107.
- [Hopkins et al. 2013] J. B. Hopkins, K. J. Lange, and C. M. Spadaccini, “Designing microstructural architectures with thermally actuated properties using freedom, actuation, and constraint topologies”, *J. Mech. Des. (ASME)* **135**:6 (2013), art. id. 061004.
- [Jefferson et al. 2009] G. Jefferson, T. A. Parthasarathy, and R. J. Kerans, “Tailorable thermal expansion hybrid structures”, *Int. J. Solids Struct.* **46**:11-12 (2009), 2372–2387.
- [Lakes 1996] R. Lakes, “Cellular solid structures with unbounded thermal expansion”, *J. Mater. Sci. Lett.* **15**:6 (1996), 475–477.
- [Lakes 2007] R. Lakes, “Cellular solids with tunable positive or negative thermal expansion of unbounded magnitude”, *Appl. Phys. Lett.* **90**:22 (2007), art. id. 221905.
- [Lehman and Lakes 2013] J. Lehman and R. Lakes, “Stiff lattices with zero thermal expansion and enhanced stiffness via rib cross section optimization”, *Int. J. Mech. Mater. Des.* **9**:3 (2013), 213–225.
- [Miller et al. 2008] W. Miller, D. S. Mackenzie, S. W. Smith, and K. E. Evans, “A generalised scale-independent mechanism for tailoring of thermal expansivity: positive and negative”, *Mech. Mater.* **40**:4-5 (2008), 351–361.
- [Phoenix and Tarazaga 2017] A. A. Phoenix and P. A. Tarazaga, “Dynamic model reduction using data-driven Loewner-framework applied to thermally morphing structures”, *J. Sound Vib.* **396** (2017), 274–288.
- [Phoenix and Tarazaga 2018] A. A. Phoenix and P. A. Tarazaga, “Thermal morphing anisogrid smart space structures, I: Introduction, modeling, and performance of the novel smart structural application”, *J. Vib. Control* **24**:13 (2018), 2853–2872.
- [Phoenix et al. 2018] A. A. Phoenix, J. Borggaard, and P. A. Tarazaga, “Thermal morphing anisogrid smart space structures, II: Ranking of geometric parameter importance, trust region optimization, and performance evaluation”, *J. Vib. Control* **24**:13 (2018), 2873–2893.
- [Sigmund and Torquato 1996] O. Sigmund and S. Torquato, “Composites with extremal thermal expansion coefficients”, *Appl. Phys. Lett.* **69**:21 (1996), 3203–3205.
- [Sigmund and Torquato 1997] O. Sigmund and S. Torquato, “Design of materials with extreme thermal expansion using a three-phase topology optimization method”, *J. Mech. Phys. Solids* **45**:6 (1997), 1037–1067.

- [Steeves et al. 2007] C. A. Steeves, S. L. dos Santos e Lucato, M. He, E. Antinucci, J. W. Hutchinson, and A. G. Evans, “Concepts for structurally robust materials that combine low thermal expansion with high stiffness”, *J. Mech. Phys. Solids* **55**:9 (2007), 1803–1822.
- [Steeves et al. 2009] C. A. Steeves, C. Mercer, E. Antinucci, M. Y. He, and A. G. Evans, “Experimental investigation of the thermal properties of tailored expansion lattices”, *Int. J. Mech. Mater. Des.* **5**:2 (2009), 195–202.
- [Toropova and Steeves 2014] M. M. Toropova and C. A. Steeves, “Bimaterial lattices with anisotropic thermal expansion”, *J. Mech. Mater. Struct.* **9**:2 (2014), 227–244.
- [Toropova and Steeves 2015] M. M. Toropova and C. A. Steeves, “Adaptive bimaterial lattices to mitigate thermal expansion mismatch stresses in satellite structures”, *Acta Astronaut.* **113** (2015), 132–141.
- [Toropova and Steeves 2016] M. M. Toropova and C. A. Steeves, “Bimaterial lattices as thermal adapters and actuators”, *Smart Mater. Struct.* **25**:11 (2016), art. id. 115030.
- [Vasiliev et al. 2012] V. V. Vasiliev, V. A. Barynin, and A. F. Razin, “Anisogrid composite lattice structures: development and aerospace applications”, *Compos. Struct.* **94**:3 (2012), 1117–1127.
- [Wei et al. 2016] K. Wei, H. Chen, Y. Pei, and D. Fang, “Planar lattices with tailorable coefficient of thermal expansion and high stiffness based on dual-material triangle unit”, *J. Mech. Phys. Solids* **86** (2016), 173–191.
- [Wei et al. 2017] K. Wei, Y. Peng, W. Wen, Y. Pei, and D. Fang, “Tailorable thermal expansion of lightweight and robust dual-constituent triangular lattice material”, *J. Appl. Mech. (ASME)* **84**:10 (2017), art. id. 101006.
- [Wei et al. 2018a] K. Wei, Y. Peng, K. Wang, S. Duan, X. Yang, and W. Wen, “Three dimensional lightweight lattice structures with large positive, zero and negative thermal expansion”, *Compos. Struct.* **188** (2018), 287–296.
- [Wei et al. 2018b] K. Wei, Q. Yang, B. Ling, Z. Qu, Y. Pei, and D. Fang, “Design and analysis of lattice cylindrical shells with tailorable axial and radial thermal expansion”, *Extreme Mech. Lett.* **20** (2018), 51–58.
- [Xu and Pasini 2016] H. Xu and D. Pasini, “Structurally efficient three-dimensional metamaterials with controllable thermal expansion”, *Sci. Rep.* **6** (2016), art. id. 34924.
- [Yousefiani et al. 2009a] A. Yousefiani, J. M. Comfort, J. G. Vollmer, and M. L. Hand, “Joined composite structures with a graded coefficient of thermal expansion for extreme environment applications”, US Patent application US20090266870A1, Boeing, 2009, <https://tinyurl.com/yb7bsgm2>.
- [Yousefiani et al. 2009b] A. Yousefiani, J. G. Vollmer, M. L. Hand, and J. M. Comfort, “Built-up composite structures with a graded coefficient of thermal expansion for extreme environment applications”, US Patent application US20090269497A1, Boeing, 2009, <https://patents.google.com/patent/US20090269497>.

Received 27 Nov 2018. Revised 3 Jan 2019. Accepted 17 Jan 2019.

MARINA M. TOROPOVA: marina.toropova@mtmedi.com
MT Medi Corp, Toronto, ON, Canada

JOURNAL OF MECHANICS OF MATERIALS AND STRUCTURES

msp.org/jomms

Founded by Charles R. Steele and Marie-Louise Steele

EDITORIAL BOARD

ADAIR R. AGUIAR	University of São Paulo at São Carlos, Brazil
KATIA BERTOLDI	Harvard University, USA
DAVIDE BIGONI	University of Trento, Italy
MAENGHYO CHO	Seoul National University, Korea
HUILING DUAN	Beijing University
YIBIN FU	Keele University, UK
IWONA JASIUK	University of Illinois at Urbana-Champaign, USA
DENNIS KOCHMANN	ETH Zurich
MITSUTOSHI KURODA	Yamagata University, Japan
CHEE W. LIM	City University of Hong Kong
ZISHUN LIU	Xi'an Jiaotong University, China
THOMAS J. PENCE	Michigan State University, USA
GIANNI ROYER-CARFAGNI	Università degli studi di Parma, Italy
DAVID STEIGMANN	University of California at Berkeley, USA
PAUL STEINMANN	Friedrich-Alexander-Universität Erlangen-Nürnberg, Germany
KENJIRO TERADA	Tohoku University, Japan

ADVISORY BOARD

J. P. CARTER	University of Sydney, Australia
D. H. HODGES	Georgia Institute of Technology, USA
J. HUTCHINSON	Harvard University, USA
D. PAMPLONA	Universidade Católica do Rio de Janeiro, Brazil
M. B. RUBIN	Technion, Haifa, Israel

PRODUCTION production@msp.org

SILVIO LEVY Scientific Editor


Cover photo: Ev Shafir

See msp.org/jomms for submission guidelines.

JoMMS (ISSN 1559-3959) at Mathematical Sciences Publishers, 798 Evans Hall #6840, c/o University of California, Berkeley, CA 94720-3840, is published in 10 issues a year. The subscription price for 2019 is US \$635/year for the electronic version, and \$795/year (+\$60, if shipping outside the US) for print and electronic. Subscriptions, requests for back issues, and changes of address should be sent to MSP.

JoMMS peer-review and production is managed by EditFLOW® from Mathematical Sciences Publishers.

PUBLISHED BY

 **mathematical sciences publishers**
nonprofit scientific publishing

<http://msp.org/>

© 2019 Mathematical Sciences Publishers

The role of rheology in modelling elastic waves with gas bubbles in granular fluid-saturated media	ADHAM A. ALI and DMITRY V. STRUNIN	1
Some general theorems for local gradient theory of electrothermoelastic dielectrics	OLHA HRYTSYNA and HALYNA MOROZ	25
Effect of surface elasticity on stress intensity factors near mode-III crack tips	XIAN-FANG LI	43
Analytical investigation of free vibrations of a bounded nonlinear bulk-elastic medium in a field of mass forces	EUGENE I. RYZHAK and SVETLANA V. SINYUKHINA	61
A modified shear-lag model for prediction of stress distribution in unidirectional fibrous composites considering interphase	MOHAMMAD HASSAN ZARE and MEHDI MONDALI	97
Nonlinear free vibration of nanobeams based on nonlocal strain gradient theory with the consideration of thickness-dependent size effect	WEI CHEN, LIN WANG and HU-LIANG DAI	119
Energy-maximizing holes in an elastic plate under remote loading	SHMUEL VIGDERGAUZ and ISAAC ELISHAKOFF	139
Anisotropic multimaterial lattices as thermal adapters	MARINA M. TOROPOVA	155
Thermal stress around an elliptic hole weakened by electric current in an infinite thermoelectric plate	KUN SONG, HAO-PENG SONG, PETER SCHIAVONE and CUN-FA GAO	179